Ferrite effects on the hydrogen embrittlement of 17-4PH stainless steel

Yaojie Zheng, Huili Sun, Luchun Yan and Huisheng Yang
School of Materials Science and Engineering, University of Science and Technology Beijing, Beijing, China
Kewei Gao and Xiaolu Pang
School of Materials Science and Engineering, University of Science and Technology Beijing, Beijing, China and Beijing Advanced Innovation Center for Materials Genome Engineering, University of Science and Technology Beijing, Beijing, China, and
Alex A. Volinsky
Department of Mechanical Engineering, University of South Florida, Tampa, Florida, USA

Abstract

Purpose – The purpose of this study is to investigate the effect of ferrite on hydrogen embrittlement (HE) of the 17-4PH stainless steels.

Design/methodology/approach – The effects of ferrite on HE of the 17-4PH stainless steels were investigated by observing microstructure and conducting slow-strain-rate tensile tests and hydrogen permeability tests.

Findings – The microstructure of the ferrite-bearing sample is lath martensite and banded ferrite, and the ferrite-free sample is lath martensite. After hydrogen charging, the plasticity of the two steels is significantly reduced, along with the tensile strength of the ferrite-free sample. The HE susceptibility of the ferrite-bearing sample is significantly lower than the ferrite-free steel, and the primary fracture modes gradually evolved from typical dimple to quasi-cleavage and intergranular cracking. After aging at 480°C for 4 h and hydrogen charging for 12 h, the 40.9% HE susceptibility of ferrite-bearing samples was the lowest. In addition, the hydrogen permeation tests show that ferrite is a fast diffusion channel for hydrogen, and the ferrite-bearing samples have higher effective hydrogen diffusivity and lower hydrogen concentration.

Originality/value – There are a few studies of the ferrite effect on the HE properties of martensitic precipitation hardening stainless steel.

Keywords 17-4PH stainless steel, Ferrite, Slow-strain-rate tensile test, Hydrogen charging, Hydrogen embrittlement susceptibility

Paper type Research paper

1. Introduction

The 17-4PH(0Cr17Ni4Cu4Nb) steel is a low carbon martensitic precipitation hardening stainless steel developed based on the Cr17 martensitic stainless steel. Due to its good mechanical properties, corrosion resistance and high-temperature resistance and relatively simple heat treatment process, it is widely used in aerospace (Chien and Tsai, 2003; Raj *et al.*, 2007), marine applications (Arisoy *et al.*, 2003) and nuclear power generation (Christien *et al.*, 2003; Wang *et al.*, 2006). However, hydrogen embrittlement (HE) is a major challenge limiting the application of ultra-high-strength martensitic stainless steels. The martensitic microstructure is very susceptible to HE, which increases with strength. Very low hydrogen concentration may cause delayed fracture without warning (Figueroa and Robinson, 2010; Li *et al.*, 2010; Li *et al.*, 2017; Venezuela *et al.*, 2018; Wang *et al.*, 2013; Zhu *et al.*, 2014). A lot of research has been conducted regarding the hydrogen embrittlement behavior of high-strength steels. Based on the observed local hydrogen concentration, researchers believe that HE in lath martensitic steels is mainly the result of combined effects of hydrogen-enhanced decohesion and hydrogen-enhanced localized plasticity (HELP) (Li *et al.*, 2018; Djukic *et al.*, 2015; Novak *et al.*, 2010).

The microstructure of steel is one of the important factors affecting HE (Venezuela *et al.*, 2016). In recent years, the research on improving the resistance to HE of martensitic stainless steel mainly focused on adding trace alloying elements, such as Nb, V and Ti, to promote the formation of carbide or nitride precipitates, thereby introducing hydrogen traps to reduce HE susceptibility (Chen *et al.*, 2017; Chen *et al.*, 2020; Cho *et al.*, 2018; Kim *et al.*, 2018; Kim *et al.*, 2021; Yang *et al.*, 2016). Kim *et al.* (2018) observed that TiC precipitation enhanced the HE susceptibility of martensitic stainless steel. Cho *et al.* (2018) reported that the precipitation of V-containing carbides in martensitic stainless steel reduced its HE susceptibility. Chen *et al.* (2017) and Chen *et al.* (2020) performed atom probe tomography analysis of deuterium-bearing samples by isotopic substitution and found that deuterium atoms were enriched in the core of V-Mo-Nb carbide and at the interface between NbC and ferrite. In addition, Yang *et al.* (2016) and Kim *et al.* (2021) showed that

The current issue and full text archive of this journal is available on Emerald Insight at: **https://www.emerald.com/insight/0003-5599.htm**

Anti-Corrosion Methods and Materials
69/3 (2022) 331–338
 [ISSN 0003-5599]
[DOI 10.1108/ACMM-03-2022-2615]

This research was financially supported by the Basic and Applied Basic Research Major Project of Guangdong Province, China (2019B030302011) and the National Natural Science Foundation of China (51971034 and 51771026).

Received 10 March 2022
Revised 14 March 2022
Accepted 16 March 2022

an appropriate amount of austenite has a positive effect on the HE resistance of martensitic stainless steels.

Ferrite is a soft phase with a higher hydrogen diffusion rate and lower hydrogen solubility than martensite, and only higher hydrogen content can cause HE fracture of ferrite-bearing materials (Loidl *et al.*, 2011; Michler and Naumann, 2010; Solheim and Solberg, 2013). Zhao *et al.* (2002) showed that acicular ferrite and ultrafine ferrite have good resistance to HE and good mechanical properties. Matsuno *et al.* (2014) and Yang *et al.* (2018) found that adding ferrite into high-strength steels can absorb part of the plastic deformation energy and reduce the stress concentration caused by martensitic transformation, thereby reducing the HE susceptibility. However, the microstructure refined by low-temperature annealing can trap more hydrogen atoms at the interface (Yang *et al.*, 2018). Ferrite has also been studied in dual-phase steels containing the ferrite phase (Bollinger *et al.*, 2019; Garcia *et al.*, 2015; Liu *et al.*, 2018).

However, there are a few studies of the ferrite effects on the HE properties of martensitic precipitation hardening stainless steels. This paper studied the effects of ferrite on HE of 17-4PH stainless steel. Using the 17-4PH stainless steel with ferrite and without ferrite, the HE susceptibility of the hydrogen-charged samples was evaluated by the slow-strain-rate tensile (SSRT) test, and the fracture morphology was observed by scanning electron microscopy. The hydrogen permeation tests were conducted to observe the diffusion behavior of hydrogen in the sample.

2. Experiment

Two kinds of the tested 17-4PH stainless steels were ferritic steel (F-bearing, Fb for short) and nonferritic steel (F-free, Ff for short). Their chemical composition is listed in Table 1. High-temperature solution treatment (1040°C) and aging treatment (480°C) were carried out for Fb and Ff. The specific treatment process and sample numbers are listed in Table 2. After different heat treatments, $10 \times 10 \times 1$ mm^3 squares of Fb and Ff were cut for microstructure observations. First, they were polished with sandpaper, and then with diamond paste with 2.5-μm particle size to mirror surface. Then, they were cleaned and dried with acetone and anhydrous ethanol. The samples were etched with 200 mL HCl + 100 g $FeCl_3$ + 1000 mL H_2O solution (Shen *et al.*, 2017) for 25 s and then immediately cleaned with anhydrous ethanol and dried. The microstructure was observed by optical microscopy (OM, Zeiss Axio Imager.M2M).

Table 1 Chemical composition of ferritic and ferrite-free 17-4PH stainless steels, Wt.%

Specimen	C	Si	Mn	P	S	Cr	Ni	Cu	Nb
Fb	0.03	0.57	0.54	0.023	0.001	16.7	3.85	3.63	0.4
Ff	0.032	0.33	0.44	0.018	0.002	15.57	4.44	3.5	0.26

Table 2 Treatment process and specimen numbers of ferritic and ferrite-free 17-4PH stainless steels

Specimen	Solution annealing	Aging condition
Fb1	1040°C/1 h/water cooling	480°C/1 h/air cooling
Fb4		480°C/4 h/air cooling
Ff1		480°C/1 h/air cooling
Ff4		480°C/4 h/air cooling

The sample geometry used for the SSRT test is shown in Figure 1(a). Before the SSRT test, the samples were polished step by step to 2000# with sandpaper, cleaned and dried with acetone and anhydrous ethanol respectively, and the non-exposed areas were encapsulated with the silica gel. The hydrogen permeability test sample was a small $\Phi 10 \times 0.5$ (thickness) mm^3 circular piece, shown in Figure 1(b). Before the test, both sides were polished evenly step by step to 5000# with sandpaper, and one side was electroplated with Ni.

The long part of the tensile specimen was charged with hydrogen at room temperature by the electrochemical method. During the hydrogen charging process, a platinum plate was used as an anode and the specimen was used as a cathode. The hydrogen-rich solution was 0.2 mol·L^{-1} NaOH, and the current density was 0.1 mA·cm^{-2}. Hydrogen charging time was 0, 12 and 24 h, respectively. SSRT tests were conducted using the Wance/ETM machine immediately after hydrogen charging, and the strain rate was 1×10^{-5} s^{-1}. A hydrogen meter (Bruker G4 Phoenix) was used to measure the hydrogen content in the sample near the fracture area, and the fracture morphology was observed by scanning electron microscopy (SEM, Zeiss Gemini 300).

Davanathan-Stachurski's double electrolytic cell device (Devanathan and Stachurski, 1964) was used to carry out hydrogen permeation tests. The sample was installed between the hydrogen charging cell and the hydrogen expanding cell. 0.2 mol·L^{-1} NaOH solution was added to the hydrogen expanding cell, and 0.28 V constant anodic oxidation potential was applied to the reference electrode (Hg/HgO) through an electrochemical workstation, and the oxidation current curve was recorded. When the oxidation current attenuated to 2×10^{-7} A·cm^{-2}, 0.2 mol·L^{-1} NaOH + 0.22 g·L^{-1} thiourea alkaline solution was added, and a constant current with 20 mA·cm^{-2} was applied. When the oxidation current stabilized, the hydrogen charging current was interrupted. The hydrogen diffusion coefficient was calculated based on the current-time curves.

3. Results and discussion

3.1 Microstructure characterizations

Figure 2 shows the microstructure of ferritic and ferrite-free 17-4PH stainless steels with different aging treatments. The microstructure of Fb is mainly strip ferrite and lath martensite in Figure 2(a) and 2(b). The microstructure of Ff is mainly lath martensite with a clear interface in Figure 2(c) and 2(d). The grain size of martensite slightly fluctuates with aging time between 34 and 42 μm without significant changes. X-ray diffraction analysis (Rigaku SmartLab, 9 KW) was performed on Fb and Ff after different aging times, and the results are shown in Figure 3. No residual austenite was detected in Fb and Ff after different aging times, and the influence of residual austenite on Fb and Ff performance can be excluded.

Figure 1 Schematics of the specimens (mm)

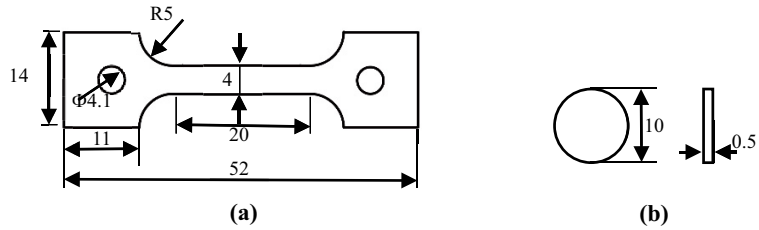

Notes: (a) Slow strain rate tensile test; (b) hydrogen permeation test

Figure 2 Microstructure of two kinds of 17-4PH stainless steels aged for 1 and 4 h

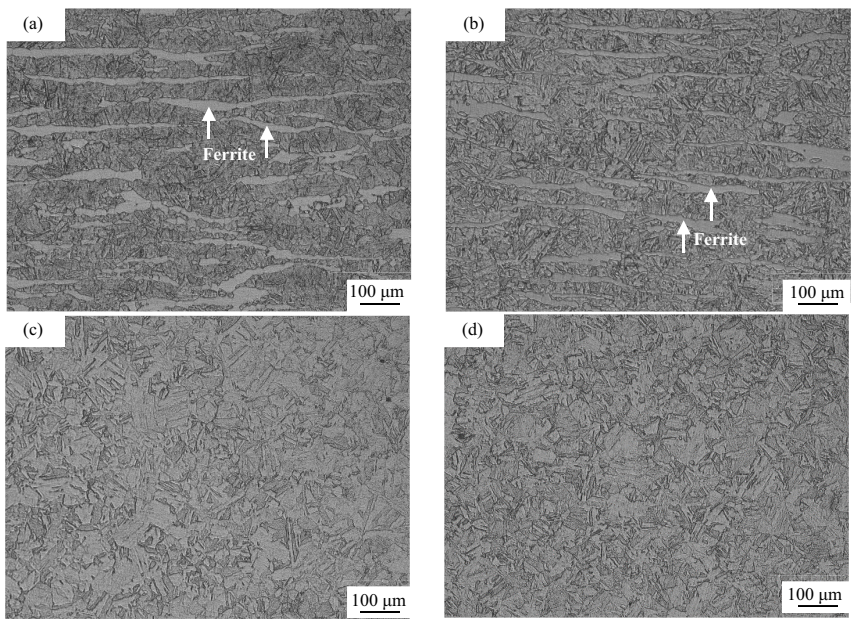

Notes: (a) Fb1; (b) Fb4; (c) Ff1; (d) Ff4

Figure 3 X-ray diffraction spectra of two kinds of the 17-4PH stainless steel aged for 1 and 4 h

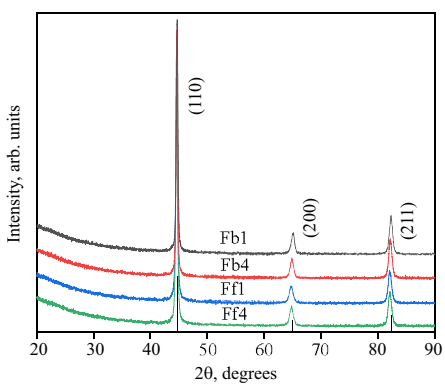

3.2 Mechanical properties

Figure 4 shows the engineering stress-strain curves of the ferritic and ferrite-free 17-4PH stainless steels after hydrogen charging for 0, 12 and 24 h. The elongation of the samples after hydrogen charging is greatly reduced. Figure 5 shows the tensile strength (σ_b) and elongation (δ) of the ferritic and ferrite-free steels as functions of hydrogen charging time. The corresponding mechanical properties and HE susceptibility (I_{HE}) are listed in Table 3. The HE susceptibility of the material was characterized by the hydrogen-induced ductility loss method. I_{HE} is used to represent the HE susceptibility index, which is calculated as:

$$I_{HE} = \frac{\delta_0 - \delta_t}{\delta_0} \times 100\% \quad (1)$$

where δ_0 and δ_t are tensile elongation of no hydrogen charging and hydrogen charged specimens, respectively.

The tensile strength of Fb is slightly lower than Ff, while the elongation of Fb is higher after the same heat treatment, indicating that the presence of ferrite can improve the ductility of the material. After hydrogen charging, the strength of the material decreases. The tensile strength decreases with hydrogen charging time in Figure 5(a). According to the principle of hydrogen charging at the cathode, hydrogen

Figure 4 SSRT engineering stress-strain curves of two kinds of 17-4PH stainless steels hydrogen charged for 0, 12 and 24 h

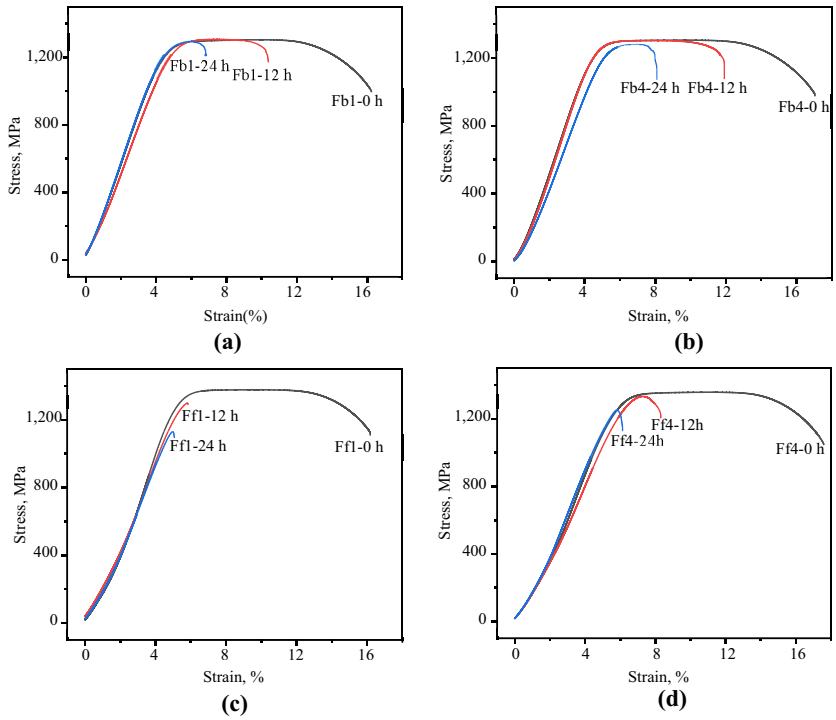

Notes: (a) Fb1; (b) Fb4; (c) Ff1; (d) Ff4

Figure 5 (a) Tensile strength and (b) elongation of two kinds of 17-4PH stainless steels with different hydrogen charging time

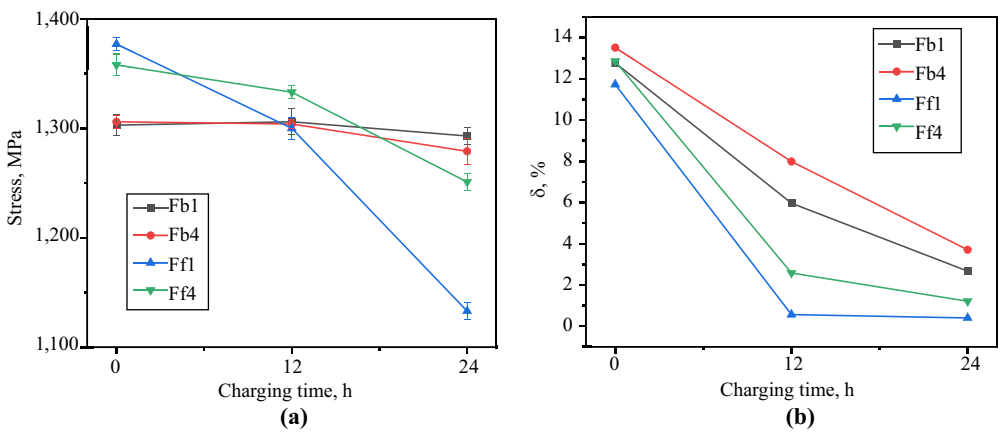

evolution reaction on the cathode sample surface increases with hydrogen charging time at constant temperature (Bai *et al.*, 2020). More hydrogen atoms are absorbed and diffused into the sample matrix with hydrogen charging time, resulting in higher hydrogen content (Devanathan and Stachurski, 1964). Due to the aggregation of a large number of hydrogen atoms, resulting in high HE susceptibility, both tensile strength and elongation decrease with hydrogen charging time. Under the same aging and hydrogen charging conditions, the tensile strength of Ff1 and Ff4 decreases significantly with hydrogen charging time, while the tensile strength of Fb1 and Fb4 changes slightly with hydrogen charging time. Therefore, the introduction of ferrite is beneficial to maintain the good mechanical properties of the 17-4PH stainless steel.

The curve of hydrogen content and HE susceptibility near the fracture area of the samples versus hydrogen charging time is shown in Figure 6. Under different aging conditions, the HE susceptibility of Ff1 is the highest, Ff4 is the second and Fb4 is the lowest. Elongation loss of Fb4 with hydrogen charging for 12 h was only 40.9% as seen in Figure 6(a), exhibiting the lowest HE susceptibility compared with Fb1 (53.29%), Ff4 (79.94%) and Ff1 (95.23%). The HE susceptibility of Fb1

Table 3 Mechanical properties of ferritic and ferrite-free 17-4PH stainless steels with different aging and hydrogen charging times at room temperature

Specimen	Hydrogen charging time, h	$\sigma_{0.2}$, MPa	σ_b, MPa	δ, %	I_{HE}, %
Fb1	0	1152	1303	12.78	–
	12	1159	1306	5.97	53.29
	24	1163	1293	2.67	79.11
Fb4	0	1187	1306	13.52	–
	12	1207	1304	7.99	40.9
	24	1185	1279	3.71	72.56
Ff1	0	1272	1377	11.73	–
	12	1246	1300	0.56	95.23
	24	1133	1133	0.4	96.59
Ff4	0	1210	1358	12.86	–
	12	1225	1333	2.58	79.94
	24	1199	1251	1.21	90.59

Figure 6 (a) Hydrogen embrittlement susceptibility and (b) hydrogen concentration of two kinds of 17-4PH stainless steels hydrogen charged for 12 and 24 h

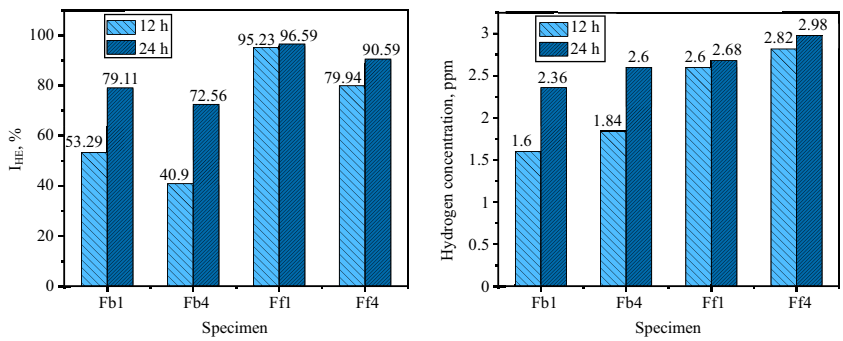

(72.93%) and Fb4 (72.56%) was also lower than Ff1 (96.59%) and Ff4 (90.59%) after 24 h hydrogen charging. Ferrite in Fb is beneficial to reduce HE susceptibility. At the same time, the hydrogen content of the samples of the two kinds of 17-4PH stainless steels after 4 h of aging treatment was greater than after 1 h of aging treatment, but the HE susceptibility of the samples after 4 h aging treatment was lower than after 1 h aging treatment, as shown in Figure 6. These results indicate that there are many deep hydrogen traps in the two 17-4PH stainless steels aged for 4 h. During the tensile test, the diffused hydrogen will be captured by hydrogen traps again, which can further reduce the HE susceptibility of the samples by prolonging the aging treatment time.

3.3 Fractography characterization

Figure 7 shows the variations in the fractured surfaces of Fb and Ff with different aging time and hydrogen charging time. The fracture mechanism changes from ductile to brittle fracture with the hydrogen charging time. Figure 7(a_1), (b_1), (c_1) and (d_1) show the fracture morphology of Fb1, Fb4, Ff1 and Ff4 samples, respectively, with no hydrogen charging, exhibiting typical dimple characteristics. When the hydrogen charging time is 12 h, both Fb1 and Ff1 show quasi-cleavage (QC) morphology and contain a small number of dimples, as shown in Figure 7(a_2) and (c_2). The difference is that Fb1 has fewer QC regions than Ff1 and includes more and deeper dimples. Fb4 has low HE susceptibility when hydrogen charging time is 12 h (Table 3), and its dimples are large and shallow, with a small amount of QC, as seen in Figure 7(b_2). However, brittle intergranular (IG) fracture occurs on the outer edge of Ff4, while ductility remains in the central region, as shown in Figure 7(d_2). During 24 h hydrogen charging, Fb absorbs more hydrogen, and the fracture characteristics change significantly, as seen in Figure 7(a_3) and (b_3). The surface of Fb1 and Fb4 is mainly characterized by the IG fracture, while the surface of Ff1 presents IG fracture in Figure 7(c_3). The outer edge of Ff4 increases in the IG fracture region, and the middle part presents a shear lip in Figure 7(d_3). Various ductile behavior can be observed along the grain plane, indicating that the fracture mechanism of lath martensitic steel is HELP-assisted fracture at a certain hydrogen concentration (Lovicu *et al.*, 2012; Michler and Naumann, 2010).

3.4 Hydrogen permeation results and quantitative analysis

Figure 8(a) shows the normalized hydrogen osmotic current density curve with a time of the ferritic and ferrite-free 17-4PH stainless steels. The apparent permeability ($\mathcal{J}_\infty L$), effective hydrogen diffusivity (D_{eff}) and diffusion hydrogen concentration (C_{app}) were calculated using equations (2)–(4):

Figure 7 SEM images of fracture surfaces of two kinds of 17-4PH stainless steels with different hydrogen charging times at the center position of the cross-sectional area at 0 h hydrogen charging

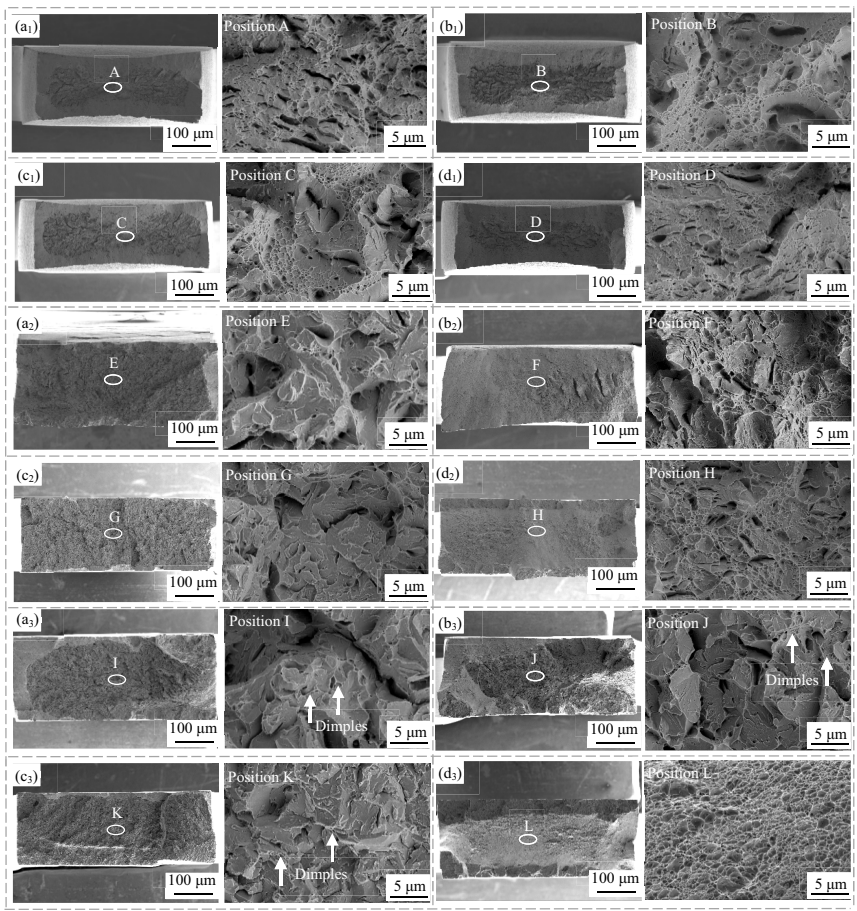

Notes: (a2) Fb1; (b2) Fb4; (c2) Ff1; (d2) Ff4; 24 h hydrogen charging: (a3) Fb1; (b3) Fb4; (c3) Ff1; (d3) Ff4

Figure 8 (a) Hydrogen permeation curves and (b) effective hydrogen diffusivity of the two kinds of 17-4PH stainless steels with different hydrogen charging and aging times

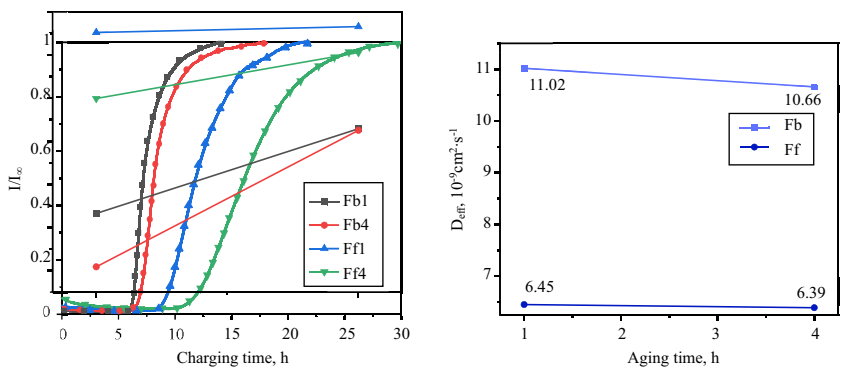

$$\mathcal{J}_{\infty}L = \frac{I_{\infty}L}{FS} \tag{2}$$

$$D_{eff} = \frac{L^2}{6t_{0.63}} \tag{3}$$

Table 4 Apparent diffusion coefficient of the ferritic and ferrite-free steels aged for 1 and 4 h

Specimen	$J_\infty L \times 10^{-12}$, mol·cm^{-1}s^{-1}	$D_{eff} \times 10^{-9}$, cm^2·s^{-1}	$C_{app} \times 10^{-4}$, mol·cm^{-3}
Fb1	3.96	11.02	3.59
Fb4	2.91	10.66	2.73
Ff1	2.48	6.45	3.85
Ff4	1.83	6.39	2.86

$$C_{app} = \frac{J_\infty L}{D_{eff}} \quad (4)$$

where I_∞(A) is the steady-state current, L (m) is the sample thickness, F is the Faraday's constant, S is the tested surface area (7.85E-5 m^2) and $t_{0.63}$(s) is the lag time defined as 0.63 times the steady-state value (Dong *et al.*, 2009; Mohtadi-Bonab *et al.*, 2014).

Relevant calculated results from hydrogen permeation tests are listed in Table 4. The effective hydrogen diffusivity of Fb1 and Fb4 is higher than Ff1 and Ff4 because hydrogen has a higher diffusion rate in ferrite than in martensite, so the introduction of ferrite can improve the hydrogen diffusion rate in steel (Loidl *et al.*, 2011; Michler and Naumann, 2010; Solheim and Solberg, 2013). At the same time, the effective hydrogen diffusivity decreases with the aging time in ferritic and ferrite-free 17–4PH stainless steels, which show the same trend of HE susceptibility, and the opposite trend of hydrogen content in the sample. However, the effective hydrogen diffusivity of Fb decreased more, as shown in Figure 8(b), indicating that the effective hydrogen diffusivity of Fb containing ferrite was greatly affected by the aging time.

Based on the above results, it is confirmed that ferrite in Fb has a positive effect on reducing the HE susceptibility of the 17–4PH stainless steel. However, ferritic 17-4PH stainless steel exhibits better HE resistance at higher effective hydrogen diffusivity and lower diffused hydrogen concentration. This is different from Shen *et al.* (2017) finding that the 17-4PH stainless steel samples exhibit better HE resistance at lower effective hydrogen diffusivity and higher diffused hydrogen concentration. The solubility of hydrogen in bcc ferrite is very low and the diffusion rate is very high (Loidl *et al.*, 2011; Michler and Naumann, 2010; Solheim and Solberg, 2013). Therefore, the ability of ferrite to improve the HE resistance of the 17-4PH stainless steel can be related to its ability to absorb part of plastic deformation work and reduce the stress concentration caused by martensitic transformation (Matsuno *et al.*, 2014; Yang *et al.*, 2018).

4. Conclusions

- After solid solution and aging treatment, the martensite in Fb and Ff is in the lath form, and the ferrite in Fb is in the form of band distribution, the grain size is 34–42 μm, and no retained austenite is found.
- With the increase of hydrogen charging time, the fracture surface of Fb and Ff evolves from dimple to quasi-cleavage, and then to intergranular. Fb has a longer transition period.
- Hydrogen charging reduces the plasticity of Fb and Ff. Compared with Ff, Fb has higher effective hydrogen diffusivity and lower diffused hydrogen concentration, but its HE susceptibility is lower than Ff, which is similar to ferrite. It has good plasticity and can relieve the stress concentration caused by martensite.

References

Arisoy, C.F., Başman, G. and Şeşen, M.K. (2003), "Failure of a 17-4PH stainless steel sailboat propeller shaft", *Engineering Failure Analysis*, Vol. 10 No. 6, pp. 711-717.

Bai, P.P., Zhou, J., Luo, B.W., Zheng, S.Q., Wang, P.Y. and Tian, Y. (2020), "Hydrogen embrittlement of X80 pipeline steel in H2S environment: effect of hydrogen charging time, hydrogen-trapped state and hydrogen charging–releasing–recharging cycles", *International Journal of Minerals, Metallurgy and Materials*, Vol. 27 No. 1, pp. 63-73.

Bollinger, A.L., Murakami, T., Findley, K.O., De Moor, E. and Speer, J.G. (2019), "The influence of microstructural variations on hydrogen absorbance and tensile properties at elevated hydrogen levels for TRIP-aided bainitic ferrite steels", *Corrosion*, Vol. 75 No. 8, pp. 888-897.

Chen, Y.S., Haley, D., Gerstl, S.S.A., London, A.J., Sweeney, F., Wepf, R.A., Rainforth, W.M., Bagot, P.A.J. and Moody, M.P. (2017), "Direct observation of individual hydrogen atoms at trapping sites in a ferritic steel", *Science (American Association for the Advancement of Science)*, Vol. 355 No. 6330, pp. 1196-1199.

Chen, Y.S., Lu, H., Liang, J., Rosenthal, A., Liu, H., Sneddon, G., McCarroll, I., Zhao, Z., Li, W., Guo, A. and Cairney, J.M. (2020), "Observation of hydrogen trapping at dislocations, grain boundaries, and precipitates", *Science*, Vol. 367 No. 6474, pp. 171-175.

Chien, W. and Tsai, C. (2003), "The investigation on the prediction of tool wear and the determination of optimum cutting conditions in machining 17-4PH stainless steel", *Journal of Materials Processing Technology*, Vol. 140 Nos 1/3, pp. 340-345.

Cho, L., Seo, E.J., Sulistiyo, D.H., Jo, K.R., Kim, S.W., Oh, J.K., Cho, Y.R. and De Cooman, B.C. (2018), "Influence of vanadium on the hydrogen embrittlement of aluminized ultra-high strength press hardening steel", *Materials Science and Engineering: A*, Vol. 735, pp. 448-455.

Christien, F., Le Gall, R. and Saindrenan, G. (2003), "Synergetic effect of hardness and phosphorus grain-boundary segregation on the ductile-to-brittle transition temperature of 17-4 PH steel", *Metallurgical and Materials Transactions. A, Physical Metallurgy and Materials Science*, Vol. 34 No. 11, pp. 2483-2491.

Devanathan, M.A.V. and Stachurski, Z. (1964), "The mechanism of hydrogen evolution on iron in acid solutions by determination of permeation rates", *Journal of the Electrochemical Society*, Vol. 111 No. 5, pp. 619-623.

Djukic, M.B., Sijacki Zeravcic, V., Bakic, G.M., Sedmak, A. and Rajicic, B. (2015), "Hydrogen damage of steels: a case study and hydrogen embrittlement model", *Engineering Failure Analysis*, Vol. 58, pp. 485-498.

Dong, C.F., Liu, Z.Y., Li, X.G. and Cheng, Y.F. (2009), "Effects of hydrogen-charging on the susceptibility of X100 pipeline steel to hydrogen-induced cracking", *International Journal of Hydrogen Energy*, Vol. 34 No. 24, pp. 9879-9884.

Figueroa, D. and Robinson, M.J. (2010), "Hydrogen transport and embrittlement in 300M and AerMet100 ultra high strength steels", *Corrosion Science*, Vol. 52 No. 5, pp. 1593-1602.

Garcia, D.C.S., Carvalho, R.N., Lins, V.F.C., Rezende, D.M. and Dos Santos, D.S. (2015), "Influence of microstructure in the hydrogen permeation in martensitic-ferritic stainless steel", *International Journal of Hydrogen Energy*, Vol. 40 No. 47, pp. 17102-17109.

Kim, J.H., Gu, G., Koo, M., Kim, E., Lee, J. and Suh, D. (2021), "Enhanced ductility of as-quenched martensite by highly stable nano-sized austenite", *Scripta Materialia*, Vol. 201.

Kim, H., Jeon, S., Yang, W., Yoo, B., Chung, Y., Ha, H. and Chung, H. (2018), "Effects of titanium content on hydrogen embrittlement susceptibility of hot-stamped boron steels", *Journal of Alloys and Compounds*, Vol. 735, pp. 2067-2080.

Li, S., Zhang, Z., Akiyama, E., Tsuzaki, K. and Zhang, B.P. (2010), "Evaluation of susceptibility of high strength steels to delayed fracture by using cyclic corrosion test and slow strain rate test", *Corrosion Science*, Vol. 52 No. 5, pp. 1660-1667.

Li, X., Zhang, J., Akiyama, E., Li, Q. and Wang, Y. (2017), "Effect of heat treatment on hydrogen-assisted fracture behavior of PH13-8Mo steel", *Corrosion Science*, Vol. 128, pp. 198-212.

Li, X., Zhang, J., Akiyama, E., Wang, Y. and Li, Q. (2018), "Microstructural and crystallographic study of hydrogen-assisted cracking in high strength PSB1080 steel", *International Journal of Hydrogen Energy*, Vol. 43 No. 37, pp. 17898-17911.

Liu, Q.L., Zhou, Q.J., Venezuela, J., Zhang, M.X. and Atrens, A. (2018) "The role of the microstructure on the influence of hydrogen on some advanced high-strength steels", *Materials Science and Engineering A – Structural Materials Properties Microstructure and Processing*, 715, pp. 370-378.

Loidl, M., Kolk, O., Veith, S. and Göbel, T. (2011), "Characterization of hydrogen embrittlement in automotive advanced high strength steels", *Materialwissenschaft Und Werkstofftechnik*, Vol. 42 No. 12, pp. 1105-1110.

Lovicu, G., Bottazzi, M., D'Aiuto, F., Sanctis, M.D., Dimatteo, A., Santus, C. and Valentini, R. (2012), "Hydrogen embrittlement of automotive advanced high-strength steels", *Metallurgical and Materials Transactions A*, Vol. 43 No. 11, pp. 4075-4087.

Matsuno, T., Sekito, Y., Sakurada, E., Suzuki, T., Kawasaki, K. and Suehiro, M. (2014), "Resistance of hydrogen embrittlement on hot-sheared surface during die-quench process", *ISIJ International*, Vol. 54 No. 10, pp. 2369-2374.

Michler, T. and Naumann, J. (2010), "Microstructural aspects upon hydrogen environment embrittlement of various bcc steels", *International Journal of Hydrogen Energy*, Vol. 35 No. 2, pp. 821-832.

Mohtadi-Bonab, M.A., Szpunar, J.A., Collins, L. and Stankievech, R. (2014), "Evaluation of hydrogen induced cracking behavior of API X70 pipeline steel at different heat treatments", *International Journal of Hydrogen Energy*, Vol. 39 No. 11, pp. 6076-6088.

Novak, P., Yuan, R., Somerday, B.P., Sofronis, P. and Ritchie, R.O. (2010), "A statistical, physical-based, micro-mechanical model of hydrogen-induced intergranular fracture in steel", *Journal of the Mechanics and Physics of Solids*, Vol. 58 No. 2, pp. 206-226.

Raj, S.V., Ghosn, L.J., Lerch, B.A., Hebsur, M., Cosgriff, L. M. and Fedor, J. (2007), "Mechanical properties of 17-4PH stainless steel foam panels", *Materials Science and Engineering: A*, Vol. 456 Nos 1/2, pp. 305-316.

Shen, S.C., Li, X.F., Zhang, P., Nan, Y.L., Yang, G.X. and Song, X.L. (2017), "Effect of solution-treated temperature on hydrogen embrittlement of 17-4 PH stainless steel", *Materials Science and Engineering. A, Structural Materials: properties, Microstructure and Processing*, Vol. 703, pp. 413-421.

Solheim, K.G. and Solberg, J.K. (2013), "Hydrogen induced stress cracking in supermartensitic stainless steels – stress threshold for coarse grained HAZ", *Engineering Failure Analysis*, Vol. 32, pp. 348-359.

Venezuela, J., Liu, Q., Zhang, M., Zhou, Q. and Atrens, A. (2016), "A review of hydrogen embrittlement of martensitic advanced high-strength steels", *Corrosion Reviews*, Vol. 34 No. 3, pp. 153-186.

Venezuela, J., Blanch, J., Zulkiply, A., Liu, Q., Zhou, Q., Zhang, M. and Atrens, A. (2018), "Further study of the hydrogen embrittlement of martensitic advanced high-strength steel in simulated auto service conditions", *Corrosion Science*, Vol. 135, pp. 120-135.

Wang, G., Yan, Y., Li, J., Huang, J., Su, Y. and Qiao, L. (2013), "Hydrogen embrittlement assessment of ultra-high strength steel 30CrMnSiNi2", *Corrosion Science*, Vol. 77, pp. 273-280.

Wang, J., Zou, H., Li, C., Peng, Y., Qiu, S. and Shen, B. (2006), "The microstructure evolution of type 17-4PH stainless steel during long-term aging at 350°C", *Nuclear Engineering and Design*, Vol. 236 No. 24, pp. 2531-2536.

Yang, J., Huang, F., Guo, Z., Rong, Y. and Chen, N. (2016), "Effect of retained austenite on the hydrogen embrittlement of a medium carbon quenching and partitioning steel with refined microstructure", *Materials Science and Engineering: A*, Vol. 665, pp. 76-85.

Yang, J., Song, Y., Lu, Y., Gu, J. and Guo, Z. (2018), "Effect of ferrite on the hydrogen embrittlement in quenched-partitioned-tempered low carbon steel", *Materials Science and Engineering: A*, Vol. 712, pp. 630-636.

Zhao, M.C., Shan, Y.Y., Xiao, F.R., Yang, K. and Li, Y.H. (2002), "Investigation on the H2S-resistant behaviors of acicular ferrite and ultrafine ferrite", *Materials Letters*, Vol. 57 No. 1, pp. 141-145.

Zhu, X., Li, W., Zhao, H., Wang, L. and Jin, X. (2014), "Hydrogen trapping sites and hydrogen-induced cracking in high strength quenching and partitioning (Q&P) treated steel", *International Journal of Hydrogen Energy*, Vol. 39 No. 24, pp. 13031-13040.

Corresponding author

Huisheng Yang can be contacted at: hsyang@263.net